



Research paper

An epidermal growth factor receptor-targeted and endoplasmic reticulum-localized organic photosensitizer toward photodynamic anticancer therapy

Xuan Zhao ^a, Haixia Ma ^a, Juanjuan Chen ^a, Fengling Zhang ^b, Xiao Jia ^a, Jinping Xue ^{a,*}

^a National and Local Joint Biomedical Engineering Research Center on Photodynamic Technologies, College of Chemistry, Fuzhou University, Fuzhou, 350116, Fujian, China

^b College of Pharmaceutical Science, Zhejiang Chinese Medical University, Hangzhou, 310053, Zhejiang, China

ARTICLE INFO

Article history:

Received 3 July 2019

Received in revised form

29 July 2019

Accepted 13 August 2019

Available online 14 August 2019

Keywords:

Photodynamic therapy

Photosensitizer

Erlotinib

Endoplasmic reticulum

Anticancer

ABSTRACT

The endoplasmic reticulum (ER), as the largest organelle in eukaryotic cells, plays complex but pivotal roles in multiple intracellular metabolic functions, including biosynthesis, sensing, and signal transduction, especially in proteins folding and post-translation modification. The ER is regarded as a promising target for anticancer therapy. Based on previous tumor-targeted photodynamic therapy (PDT), we chemically modified the phthalocyanine-based photosensitizer molecule with the small molecular anticancer-targeting drug erlotinib and the ER-targetable moiety methyl sulfonamide to develop an advanced photosensitizer **EB-ER-Pc** that can specifically target the subcellular organelle ER of EGFR-overexpressing cancer cells. The in vitro experiments show that the dual-target photosensitizer **EB-ER-Pc** can generate ROS in situ in the ER of the tumor target region to induce ER stress, upregulate Ca²⁺ ion level, and decrease mitochondrial membrane potential (MMP) to mediate cancer cells death and ablation. The results suggest that **EB-ER-Pc** is a promising candidate for effective photodynamic cancer therapy.

© 2019 Elsevier Masson SAS. All rights reserved.

1. Introduction

Though diagnostic and therapeutic techniques in cancer have achieved significant advances, cancer remains one of the most serious life-threatening illnesses worldwide [1,2]. Photodynamic therapy (PDT) has been extensively recognized as a promising therapeutic modality in the battle against various kinds of cancers due to the unique advantages of intrinsically noninvasive safety, high spatiotemporal precision, and no multidrug resistance. Generally, PDT utilizes a photosensitizer (PS), intracellular molecular oxygen, and optimum light illumination to generate highly cytotoxic oxides, i.e., reactive oxygen species (ROS) [3,4]. The exogenously generated ROS can efficiently react with cellular constituents, leading to cell death and tumor ablation [5]. The effective PS is an exceptionally paramount factor during the PDT process. The small molecule organic photosensitizers have multiple advantages

over photodynamic inorganic nanomaterials including their inherent superiority of high photodynamic activities, excellent biocompatibility, and biodegradability [6]. Currently, several photosensitizers for cancer therapy have been approved by the US Food Drug Administration (FDA) [7–9]. And a variety of potential photosensitizers are under clinical trials [10]. However, despite these great advances, PDT in cancer therapy also encounters some urgent bottlenecks [3]. Especially, the current most used preclinical and clinical photosensitizers do not exhibit profound specificity to the malignant cells in the application of PDT, leading to compromised therapeutic efficiency and undesirable treatment-related side effects. To address these challenges, it is more significant to develop targeted PDT.

In recent decades, targeted PDT provides an innovative approach to improve cancer-targeting specificity and photodynamic anticancer activities [11,12]. One emerging and commonly used strategy is to chemically modify the photosensitizing agent with tumor-targeted ligands including some organic functional moieties and bioactive molecules which can bind to the receptors overexpressed in the tumor cells [13–15]. For example, we recently designed and synthesized cancer-targeted photosensitizers via

* Corresponding author. College of Chemistry, Fuzhou University, No. 2 Xueyuan Road, Fuzhou, Fujian, 350116, China.

E-mail address: xuejinpings66@fzu.edu.cn (J. Xue).

Abbreviations

ER	endoplasmic reticulum
EB	erlotinib
PDT	photodynamic therapy
PS	photosensitizer
EGFR	epidermal growth factor receptor
MMP	mitochondrial membrane potential
ROS	reactive oxygen species
SiPc	silicon (IV) phthalocyanine
DPBF	1,3-diphenylisobenzofuran
DMEM	Dulbecco's modified Eagle medium
CEL	cremophor EL
DCFH-DA	2,7-dichlorofluorescein diacetate
DCFH	2',7'-dichlorodihydro-fluorescein
DCF	2',7'-dichlorofluorescein
CLSM	confocal laser scanning microscopy
FBS	fetal bovine serum
MTT	methyl thiazolyl tetrazolium

conjugation with small-molecule anticancer drugs (erlotinib or tamoxifen) to enhance the selectivity and targeting ability to the epidermal growth factor receptor (EGFR) or estrogen receptor-overexpressing cancer cells [12,16]. These targeted photosensitizers are often referred to as the third generation photosensitizers for PDT [17]. In comparison with conventional non-targeted PDT, the targeting strategy can improve cellular uptake of photosensitizers to enhance the PDT efficiency and remarkably minimize severe side effects to normal cells and tissues. The strategy promotes the development of PDT to a certain extent. Despite it, targeted PDT still suffers from the barrier of low PDT efficacy and inadequate tumor affinity, etc. Thus, it is highly desired to develop more precise and effective photosensitizers for the PDT application.

The future precision and personalized medicine is that the drugs will be specially tailored for each patient's need and then targeted delivery to disease site but not healthy cells [18]. However, tumor cells as the target is never the end of targeted drug therapy. Very recently, organelles as the target notably received considerable interest in current cancer treatments, especially in photodynamic cancer therapy [19]. For instance, intensive efforts have been devoted to develop mitochondria-targeted therapeutics and diagnosis [6,20–23]. Organelle-targeted cancer therapy holds great promise in the age of precision and personalized medicine [24]. The endoplasmic reticulum (ER), as the largest organelle in eukaryotic cells, plays complex but pivotal roles in multiple intracellular metabolic processes, involved in biosynthesis, sensing, and signal transduction, especially in protein folding and post-translation modification [25]. Perturbations in ER function can lead to the accumulation of unfolded proteins that can trigger ER stress. Excessively generated ER stress can directly induce tumor cell death which provides a unique and promising strategy to eradicate cancer cells [26,27]. So far, the ER has been extensively studied as a target for fluorescence probes to track the level of intracellular relevant substances [28–30]. Nevertheless, the ER exerted as a target for anticancer treatments is not well documented due to its complex role in cell signaling and other reasons [26]. Meanwhile, the methyl sulfonamide group has been adequately demonstrated to be able to direct target molecules into the ER [28,31].

Herein, we designed and prepared an advanced photosensitizer that can selectively perform photodynamic treatments in the ER of EGFR-overexpressing tumor cells. In vitro experiments demonstrated that **EB-ER-Pc** shows excellent tumor-targeted specificity

and superior photodynamic anticancer activity. In addition, it was noteworthy that the unsymmetrical axially-substituted silicon (IV) phthalocyanine (SiPc) conjugates by one-pot reaction remain rarely be reported [32,33]. The unsymmetrical SiPcs provide a paradigm whereby SiPcs can be functionalized with different groups to construct dual-functional PDT agents as personalized tailored medicines.

2. Results and discussion

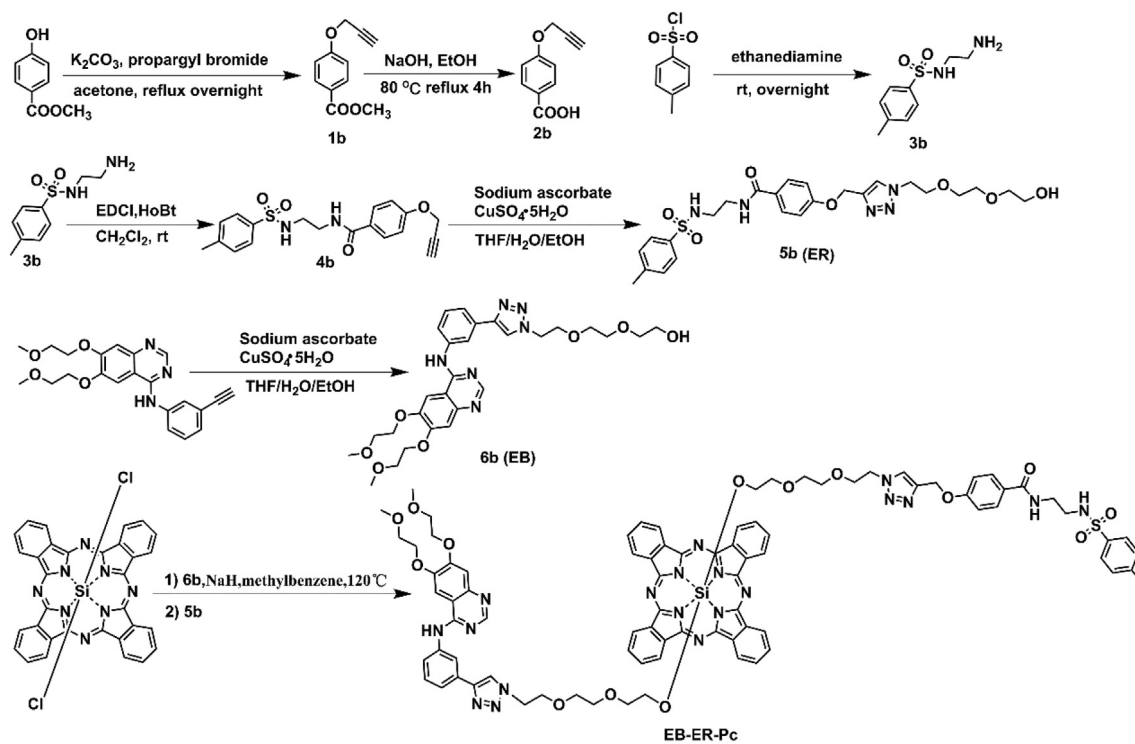
2.1. Molecular design and synthesis

As is shown in [Scheme 1](#), we employed the most promising SiPc as the photosensitizing core (**Pc**) to conjugate with the small molecule targeted drug erlotinib (**EB**). Then ER-targetable moiety methyl sulfonamide (**ER**) was then anchored on the other side of the axis via covalent attachment. The target compound was termed as **EB-ER-Pc**. The erlotinib in **EB-ER-Pc** was introduced to improve the tumor-targeted specificity. Meanwhile, the ER-targetable moiety can precisely direct it into the ER of the tumor-targeted region. In contrast, the Pcs merely conjugated with **EB** or triethylene glycol were also synthesized which were denoted as **EB-Pc** or **PEG-Pc**, respectively ([Fig. 1](#)).

[Scheme 1](#) depicts the rational design and detailed synthetic routes to prepare the target conjugate **EB-ER-Pc**. First, SiPc dichloride underwent a nucleophilic substitution reaction with **6b** in the presence of sodium hydride in anhydrous toluene. And then the intermediate was further treated with **5b**, giving the unsymmetrical axially-substituted conjugate **EB-ER-Pc**. The reference compounds **EB-Pc** and **PEG-Pc** were synthesized in a simple and similar manner. These compounds could be separated and purified readily via common column chromatography on silica gel or Al_2O_3 and were fully characterized by using NMR and HRMS (Supporting Information).

2.2. Electronic absorption and photophysical properties

The electronic absorption spectra of these designed phthalocyanine-based photosensitizers were recorded in DMF. The compounds **EB-ER-Pc**, **EB-Pc**, and **PEG-Pc** all show typical characteristic absorption spectra of monomolecular phthalocyanine with remarkably intense sharp Q and B bands ([Fig. 2](#)). And the absorption of B band strictly conforms to the Lambert-Beer law which is attached in the inset plots. Upon excitation at 610 nm, these conjugates exhibited a strong fluorescence emission ([Fig. S1](#)). The fluorescence quantum yields were calculated by using unsubstituted zinc (II) phthalocyanine (ZnPc, $\Phi_F = 0.28$ in DMF) as a reference standard. The conjugates **EB-ER-Pc** and **PEG-Pc** have similar fluorescence quantum yields about 0.39 whereas **EB-Pc** is merely 0.27. The ability of photodynamic-induced singlet oxygen generation is a great concern in the development of PDT reagents. The singlet oxygen quantum yield (Φ_{Δ}) of these conjugates were also determined by using 1,3-diphenylisobenzofuran (DPBF) as the scavenger in DMF, which was calculated relative to unsubstituted zinc (II) phthalocyanine (ZnPc, $\Phi_{\Delta} = 0.56$ in DMF) [34]. The Φ_{Δ} value of **EB-Pc** is 0.27 and is lower than **EB-ER-Pc** ($\Phi_{\Delta} = 0.39$) and **PEG-Pc** ($\Phi_{\Delta} = 0.35$) ([Fig. S2](#)). We inferred that the differences could be attributed to the different substituents on the SiPc axes. Such different substituents may affect the configurations of the photosensitizers. This may further influence the processes of energy transfer or photoinduced electron transfer (PET) between the different moieties and the sensitizer core, which leads to the changes of fluorescence and photodynamic properties of the three photosensitizers. These obtained detailed spectroscopic data were summarized in [Table S1](#).



Scheme 1. The synthetic routes of EB-ER-Pc.

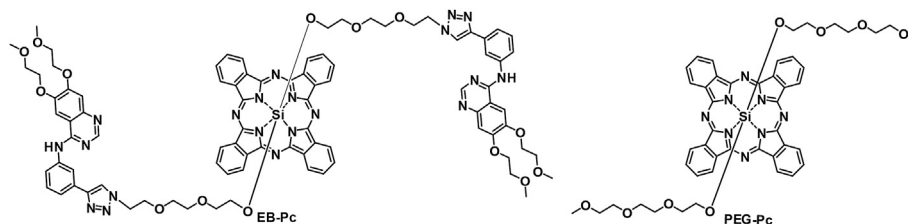


Fig. 1. The structures of EB-Pc and PEG-Pc.

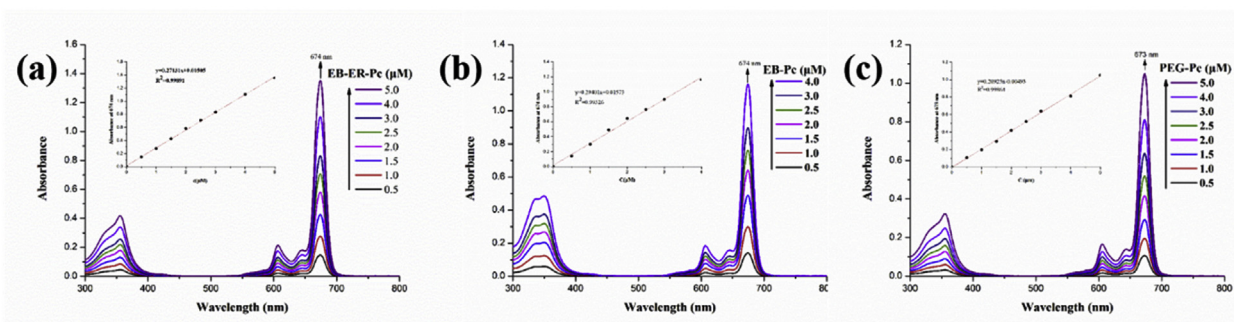


Fig. 2. UV/vis absorption spectra of EB-ER-Pc (a), EB-Pc (b), and PEG-Pc (c) in DMF at different concentrations. The inset plots of the Q-band absorbance versus the concentration of these conjugates.

Additionally, the electronic absorption spectra of these compounds were also recorded in Dulbecco's modified Eagle medium (DMEM) in the presence of 0.5% (v/v) Cremophor EL (CEL) and 1% (v/v) DMF. As is shown in Fig. 3, these conjugates also showed non-aggregated sharp peaks in DMEM existed as a monomeric phthalocyanine molecule state which is vital for effective photodynamic singlet oxygen generation in biological systems. These results

collectively confirmed that these phthalocyanine-based photosensitizers have the great promise for PDT applications.

2.3. Studies of subcellular colocalizations

The PDT-generated ROS has an extremely short half-life and diffusion radius in biological systems. This is an advantage which

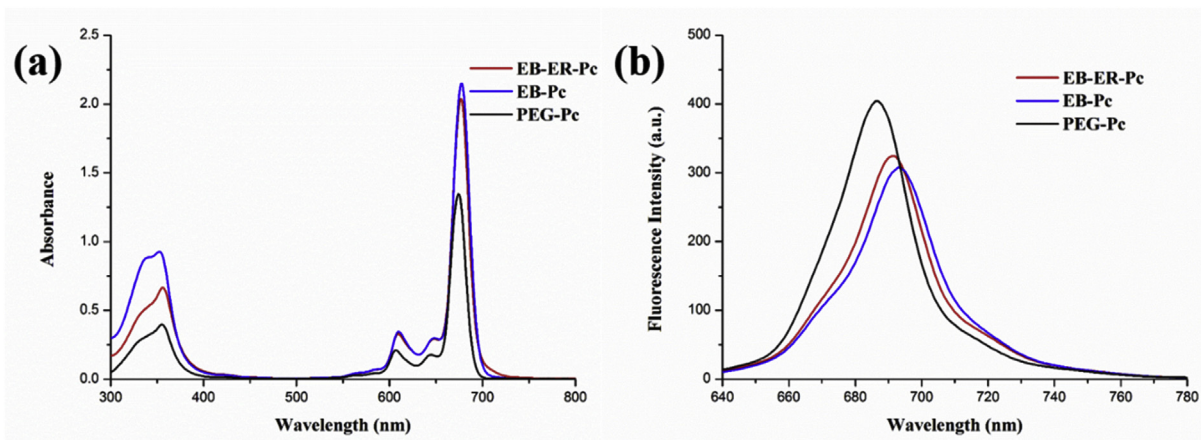


Fig. 3. The electronic absorption spectra (a) and fluorescence emission spectra (b) of **EB-ER-Pc**, **EB-Pc**, and **PEG-Pc** (all at 10 μM) in DMEM with 0.5% CEL and 1% DMF.

can effectively avoid undesired side effects but exceedingly affect the therapeutic outcomes simultaneously [35]. Hence, the subcellular localization of photosensitizers uptake by cancer cells is crucial for PDT treatment efficacy. The subcellular localization of **EB-ER-Pc**, **EB-Pc**, and **PEG-Pc** was studied by confocal laser scanning microscopy (CLSM). The A549 cells and PC-9 cells were incubated with 1.0 μM photosensitizers in the dark for 24 h, respectively. After that, the commercially available probes ER-Tracker Green, Mito-Tracker green, and Lyso-Tracker Green were utilized to analyze the intracellular detailed localization (Figs. S3–8). The Pearson's colocalization coefficient of **EB-ER-Pc** with ER-Tracker is higher than **EB-Pc** and **PEG-Pc** in two cancer lines (Fig. 4). The results reveal that **EB-ER-Pc** preferably localizes in the ER, while **EB-Pc** and **PEG-Pc** mainly concentrate in the lysosomes and mitochondria. The results clearly demonstrated that the moiety methyl sulphonamide could make **EB-ER-Pc** with ER-targetable ability.

2.4. Detection of intracellular ROS

The intracellular ROS generation ability is closely associated with the PDT efficiency. The production of intracellular ROS by the three designed photosensitizers is investigated by using a standard ROS fluorescence probe (2,7-dichlorofluorescein diacetate, DCFH-

DA). DCFH-DA can only be converted into non-fluorescent 2',7'-dichlorodihydro-fluorescein (DCFH) via the deacetylate reaction by intracellular esterase. The DCFH can then be directly oxidized by ROS to generate highly fluorescent 2',7'-dichlorofluorescein (DCF) which can radiate the characteristic green fluorescence upon excitation [36]. The ROS generating ability of **EB-ER-Pc** was first evaluated by CLSM. As is shown in Fig. 5, there was negligible green fluorescence indicating hardly ROS production in the control experiments even after light illumination. The cells displayed increasing green fluorescence in an **EB-ER-Pc** dosage-dependent manner. Particularly, the cells treated with 0.5 μM **EB-ER-Pc** showed extremely strong green fluorescence indicating massive overproduction of ROS. Moreover, quantitative analysis of the intracellular mean ROS fluorescence intensity induced by three photosensitizers was further calculated by cell lysis method (Fig. 6). The intracellular ROS levels show the concentration-dependent increase after PDT treatments. These results demonstrate that these photosensitizers have effective ROS production ability in biological systems.

2.5. Mitochondrial membrane potential assay

Mitochondria are one of the most pivotal organelles in the eukaryotic cells and take part in a vast array of cellular process [18].

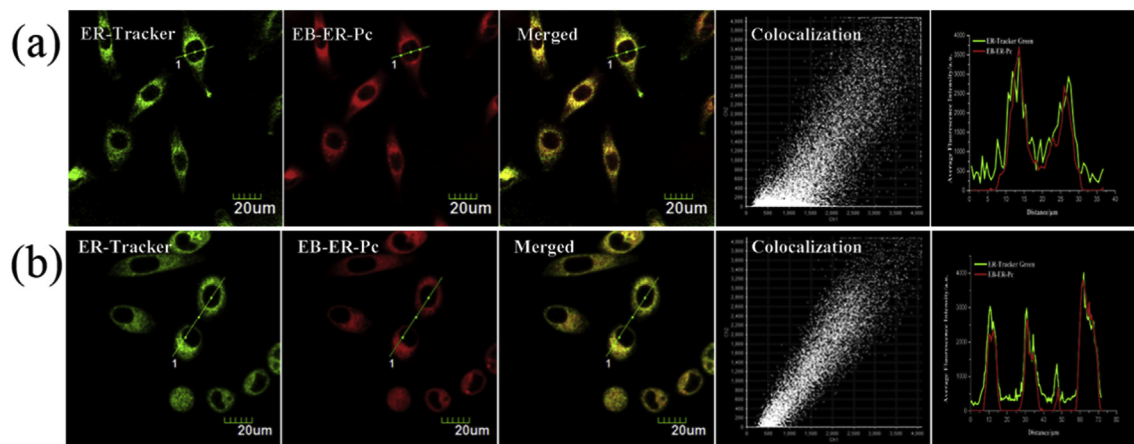


Fig. 4. Confocal fluorescence images of A549 cells (a) and PC-9 cells (b), treated with **EB-ER-Pc** (1 μM) and ER-Tracker Green (1 μM). Fluorescence intensity profiles of **EB-ER-Pc** (red line) and Tracker (green line) traced along the white lines in the merged images. (For interpretation of the references to color in this figure legend, the reader is referred to the Web version of this article.)

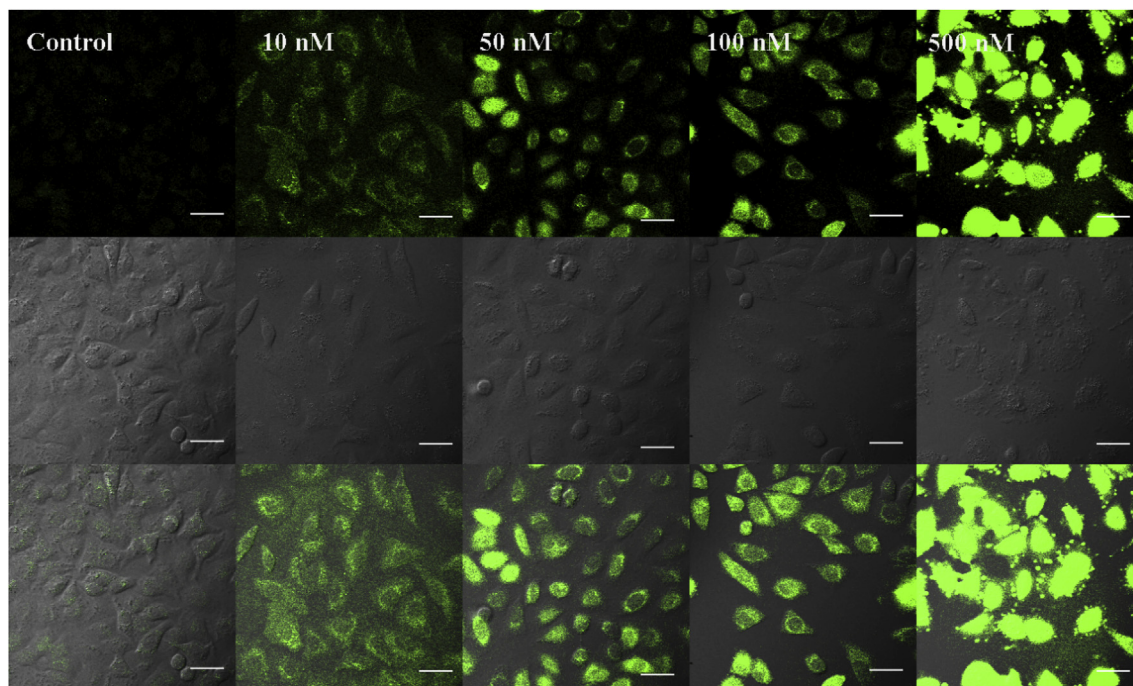


Fig. 5. Fluorescence images of intracellular ROS production by **EB-ER-Pc** in A549 cells as determined by DCFH-DA probe. The green fluorescence indicated ROS production after PDT treatment. (For interpretation of the references to color in this figure legend, the reader is referred to the Web version of this article.)

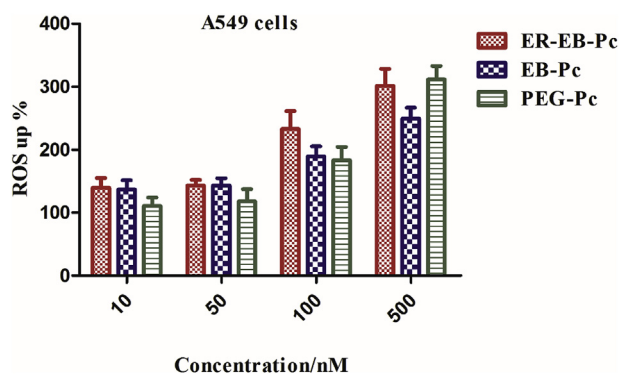


Fig. 6. Intracellular ROS production by **EB-ER-Pc**, **EB-Pc**, and **PEG-Pc** in A549 cells. The cells treated with different concentrations of three photosensitizers (10, 50, 100, and 500 nM) for PDT treatments. The intracellular ROS levels, as reflected by the fluorescence of DCFH-DA (10 μ M), after the PDT treatment with the conjugates.

As reported, mitochondria play an extremely important role in PDT-induced apoptosis [37]. The loss of mitochondrial membrane potential (MMP) is a crucial and representative mark of the apoptotic events. The generated cytotoxic ROS in the ER can immediately induce the therapeutic ER stress and indirectly decrease MMP. The commercially available fluorescence indicator JC-1 dye is generally employed to measure the MMP. In normal cellular mitochondria, JC-1 dye molecules accumulate as aggregates with red fluorescence (590 nm) relevant to high membrane potential. However, in dysfunctional mitochondria, the JC-1 dye molecules exist as a monomeric molecule coupled with green fluorescence (530 nm) due to the low membrane potential. Hence the proportion of red/green fluorescence is generally regarded as an index to investigate the status of mitochondria which can indirectly reflect the state of the cell. As is seen in Fig. 7, the cells treated without drugs or 1 nM **EB-ER-Pc** merely displayed a high ratio of red fluorescence and no detectable green fluorescence, indicating hyperpolarized

mitochondria. The cells treated with 10 or 25 nM **EB-ER-Pc** showed a higher ratio of green fluorescence than the control groups treated with **PEG-Pc** or **EB-Pc** at the same concentrations (Fig. S10). There was a bright green fluorescence and a negligible red fluorescence when the cells were treated with these three compounds at 100 nM which indicated a sharp decrease of the MMP. Consequently, we infer that **EB-ER-Pc** can generate ROS in the ER to induce ER stress and then act on mitochondria to decrease MMP at a small dose which is superior to the reference compounds.

2.6. Chromatin condensation analysis by Hoechst staining

Chromatin condensation is another typical and important mark of apoptosis following the loss of the MMP [36]. The fluorescence dye Hoechst 33258 was chosen as the fluorescence probe to observe the chromatin form changes by CLSM (Fig. 8). In the control group merely with light, the nucleus showed uniform blue fluorescence. It was found that the cells treated with **EB-ER-Pc** at 1 or 10 nM showed slight morphological changes. While the clear and obvious chromatin condensation was observed in the cells treated with 50 or 100 nM **EB-ER-Pc**. These results proved that **EB-ER-Pc** caused apoptosis correlative with treated drug concentration.

2.7. EGFR-related co-culture competitive experiments

To verify the cancer targeting specificity and affinity, we utilized two kinds of cell lines with different EGFR expression levels and obvious morphology differences, namely A549 cells (a round cancer cell line with a high expression level of EGFR) and HELF cells (a strip normal cell line with a low EGFR expression). We co-cultured these two cell lines in one confocal dish to investigate EGFR-relevant competitive uptake of conjugates by CLSM. As is shown in Fig. 9a and b, the fluorescence intensity of **EB-ER-Pc** or **EB-Pc** uptake by A549 cells was remarkably stronger than that in HELF cells. However, it was observed that there were scarcely any significant

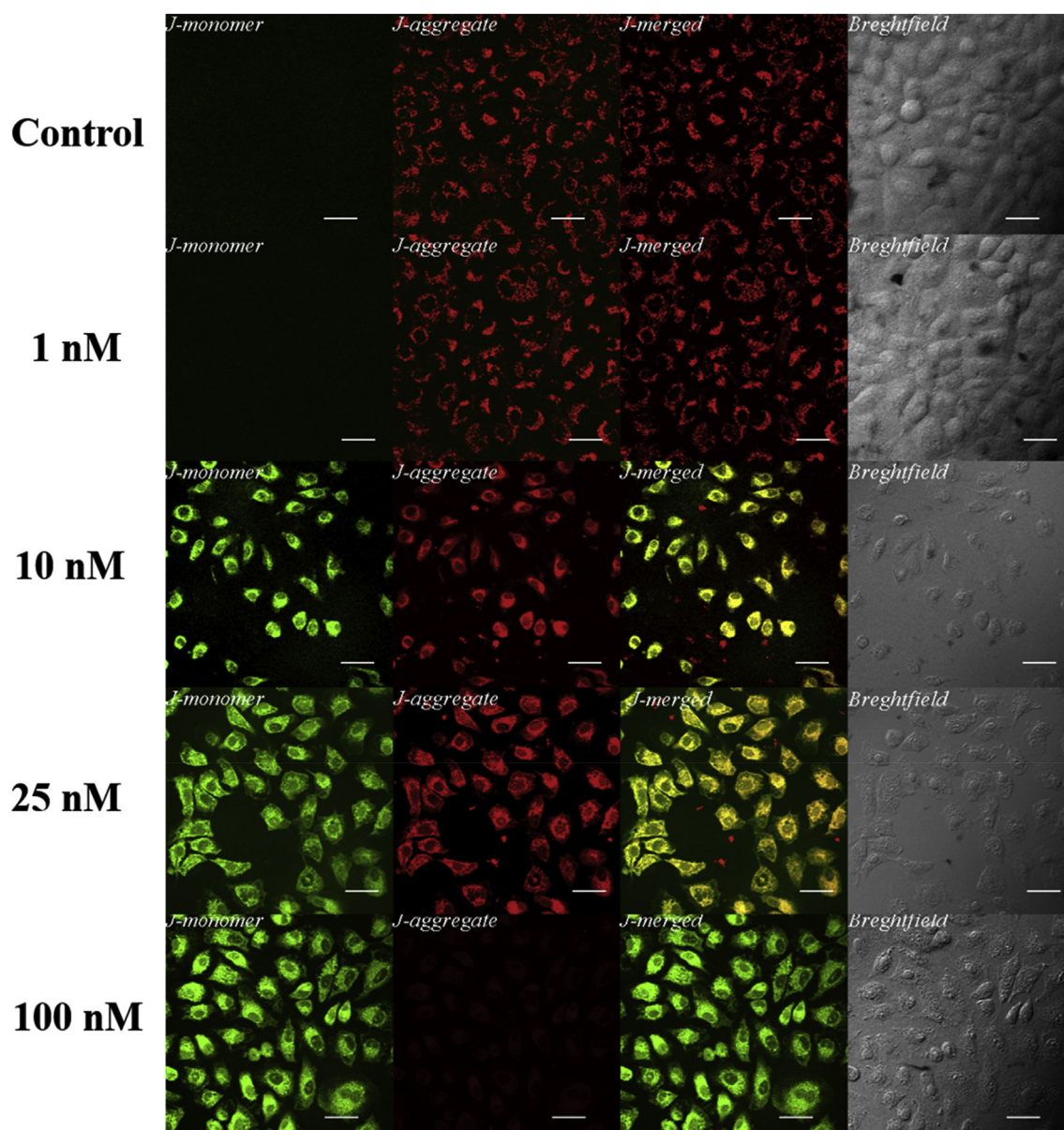


Fig. 7. The confocal microscopy fluorescence images showing the MMP of A549 cells after PDT treatments with **EB-ER-Pc** as determined by JC-1 probe. Red fluorescence indicates healthy cells with high MMP and green fluorescence represents apoptotic cells with low MMP. All the images share the same scale bar of 30 mm. (For interpretation of the references to color in this figure legend, the reader is referred to the Web version of this article.)

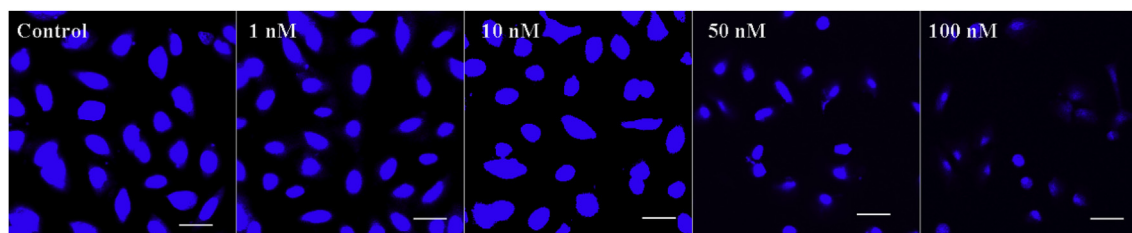


Fig. 8. The fluorescent images of Hela cells treated with **EB-ER-Pc** and stained with Hoechst 33258. All the images share the same scale bar of 30 mm.

differences in the cells incubated with **PEG-Pc** between A549 cells and HELF cells (Fig. 9c). These results demonstrated that **EB-ER-Pc** can achieve a higher uptake in the cancer cells with a high expression of EGFR owing to the introduction of targeting moiety erlotinib.

2.8. In vitro photocytotoxicity assay

The in vitro photodynamic antitumor activity of **EB-ER-Pc**, **EB-Pc**, and **PEG-Pc** was evaluated by the methyl thiazolyl tetrazolium (MTT) assays. During the process of PDT, the A549 cells, PC-9 cells,

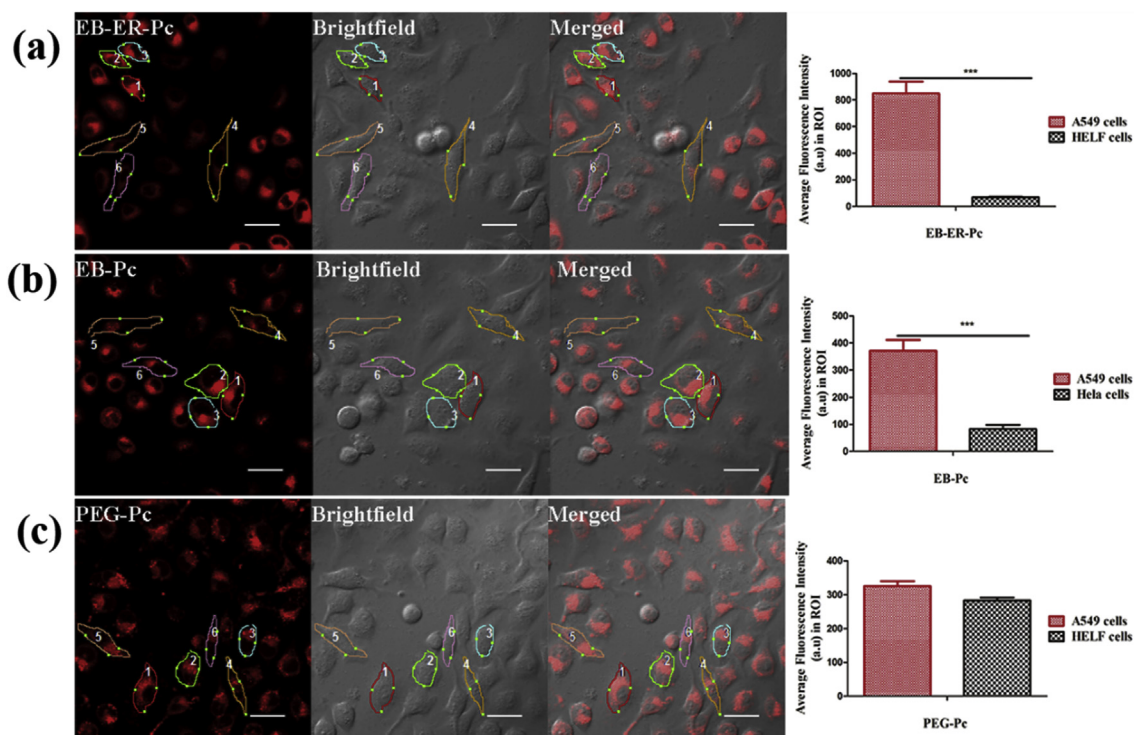


Fig. 9. Confocal fluorescence images of co-cultured A549 (round) and HELF (strip) cells after incubation with (a) **EB-ER-Pc**, (b) **EB-Pc**, and (c) **PEG-Pc** for 24 h (all at 0.5 μM) along with quantified average fluorescence intensity in A549 cells and HELF cells. All the images share the same scale bar of 30 μm . (Data are expressed as the mean \pm SD of three independent experiments. Statistical analysis: *** $p < 0.001$, ** $p < 0.01$, * $p < 0.05$.)

and HELF cells were incubated with the three phthalocyanine-based compounds at different concentrations. The IC_{50} values of **EB-ER-Pc** were as low as 6.99 nM against A549 cells and 4.20 nM against PC-9 cells which were lower than **EB-Pc** and **PEG-Pc** (Fig. 10 and Table 1). The results showed that the anticancer activity of **EB-ER-Pc** was better than the reference compounds toward tumor cell lines A549 cells and PC-9 cells. But in normal cell line HELF cells, **EB-ER-Pc** did not display the superiority compared with the reference compounds, even worse than **PEG-Pc**. The three designed final products exhibited negligible cytotoxicity against A549 cells and PC-9 cells at the same drug concentrations in the absence of light. These conjugates gradually exhibited dark cytotoxicity until 10 μM (Fig. S9). The IC_{50} values of these compounds are summarized in Table 1. The results demonstrated that **EB-ER-Pc** showed excellent photodynamic anticancer activity and extremely low dark cytotoxicity.

Furthermore, the potential photodynamic anticancer ability of the target compound **EB-ER-Pc** was further evaluated through the

Table 1

IC_{50} values for **EB-ER-Pc**, **EB-Pc**, and **PEG-Pc** against A549 cells, PC-9 cells, and HELF cells.

	IC_{50} values (nM)		
	EB-ER-Pc	EB-Pc	PEG-Pc
A549 cells	6.99	15.2	14.4
PC-9 cells	4.20	10.8	8.45
HELF cells	25.4	38.1	12.0

In the presence of light ($\lambda = 670 \text{ nm}$, 12.5 mWcm^{-2} for 2 min, 1.5 J cm^{-2}).

live/dead cells double staining (calcein AM and propidium iodide). The red fluorescence indicated dead cells and the green fluorescence indicated live cells. As shown in Fig. 11, the control group merely with light or treated with 1 nM **EB-ER-Pc** exhibited intense green fluorescence and negligible red fluorescence with hardly any dead cells. The green fluorescence gradually decreased with emerging red fluorescence when the cells were treated with 5 or

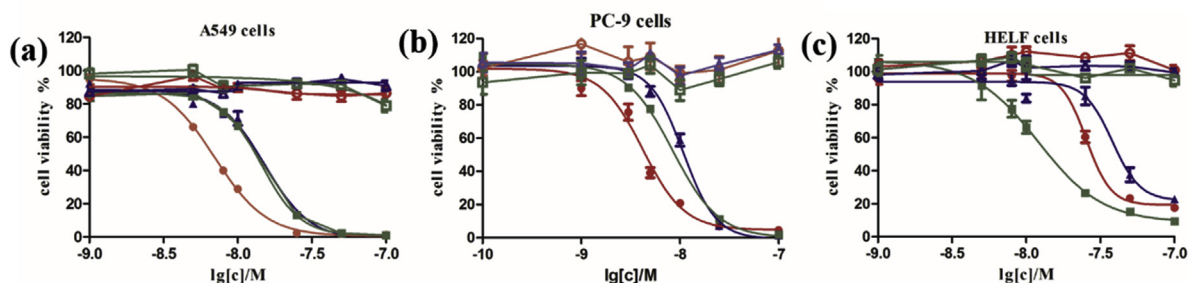


Fig. 10. The cytotoxic effects of **EB-ER-Pc** (circles), **EB-Pc** (triangles), and **PEG-Pc** (squares) on A549 cells (a), PC-9 cells (b), and HELF cells (c) in the absence (open symbols) and presence (closed symbols) of light ($\lambda = 670 \text{ nm}$, 12.5 mW cm^{-2} , 1.5 J cm^{-2}). Data are expressed as mean value \pm standard error of the mean value of three independent experiments.

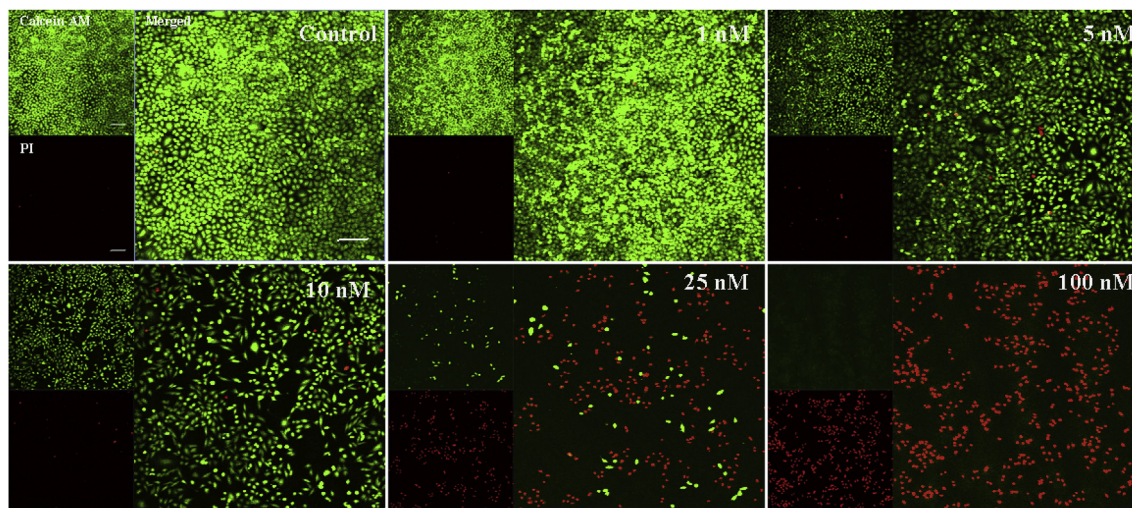


Fig. 11. Confocal fluorescence images of A549 cells stained with calcein AM/PI after PDT treatments with **EB-ER-Pc**. The live cells were dyed with green fluorescence and the dead cells were dyed with red fluorescence. All the images share the same scale bar of 150 μm . (For interpretation of the references to color in this figure legend, the reader is referred to the Web version of this article.)

10 nM **EB-ER-Pc**. It was observed that there was a myriad of red fluorescence coupled with few green fluorescence in the cells treated with 25 nM. Nearly all cells were dead at 100 nM. The red/green ratios gradually increase with **EB-ER-Pc** concentrations, which is consistent with above MTT assays.

2.9. The investigation of intracellular calcium level

As we also know, Ca^{2+} ions play key roles in multiple cellular physiological processes including cell proliferation, differentiation, and apoptosis, etc. Moreover, the ER is the major storage of intracellular Ca^{2+} and Ca^{2+} -binding chaperones that mediate the proper folding of proteins in the ER lumen. It is well established that Ca^{2+} trafficking in and out of the ER regulates a range of cellular processes as well as signaling transduction pathways relevant to ER stress response, modulation of transcriptional processes, and development. For instance, the release of Ca^{2+} from the ER can trigger many signaling mechanisms that induce cell apoptosis and necrosis mainly by means of Ca^{2+} -mediated mitochondrial cell death [38]. To visualize the changes of tumor Ca^{2+} ions level after the PDT treatments, the commercially available standard calcium ions fluorescent indicator Rhod-3 AM was employed to measure intracellular Ca^{2+} ion concentrations. The A549 cells after PDT treatments with these three photosensitizers all showed an increase of calcium ions level along with elevated drug concentrations. The experiment groups treated with **EB-ER-Pc** showed higher concentrations than the other two groups—especially the cells treated with the dose of 75 or 100 nM (see in Fig. 12). The ER stress caused by ER-localized **EB-ER-Pc** can instantly mediate Ca^{2+} level up which is more sensitive and quick than other organelles locating photosensitizers. Consequently, the intracellular photo-dynamically generated ROS and excessive Ca^{2+} synergistically induce tumor cells apoptosis and necrosis.

3. Conclusion

In summary, we designed and synthesized an advanced phthalocyanine-based organic photosensitizer **EB-ER-Pc** that can specifically localize in the ER of the EGFR-overexpressing tumor cells. The chemically modified small molecular targeted drug erlotinib can direct it into the tumor site. Once reaching the tumor

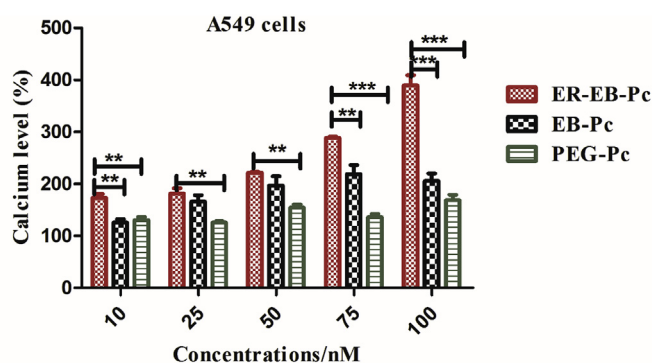


Fig. 12. The intracellular calcium level detection after the treatment with **EB-ER-Pc**, **EB-Pc**, and **PEG-Pc** in A549, respectively. The intracellular calcium level as reflected by the fluorescence of Fluo-3 AM (5.0 μM), after the treatment with these conjugates upon light illumination ($\lambda = 610 \text{ nm}$) are shown as the means with SEM of three independent experiments (* $p < 0.005$; ** $p < 0.05$; *** $p < 0.001$).

region, the anchored methyl sulfonamide moiety can lead it to the ER. The in vitro experiments demonstrated that PDT generates cytotoxic ROS in the ER that induces ER stress, upregulates intracellular Ca^{2+} ions level, and decreases MMP to accelerate tumor cells death in a synergistic manner. Compared to non-targeted or tumor-targeted PDT, **EB-ER-Pc** exhibits a superior photodynamic tumor ablation ability than reference compounds, **EB-Pc** and **PEG-Pc**. The strategy achieves a more precise and personalized treatment modality that the photosensitizer can selectively perform PDT in the ER of the tumor-targeted sites. To the best of our knowledge, this is the first report of a tumor and ER dual-targeted organic photosensitizer. We believe that our work is more significant to provide a promising strategy for designing the advanced photosensitizers, especially in the ER-targeted photosensitizing agents, in the current era of precise and personalized medicine.

4. Experimental

4.1. General

Materials: The used methylbenzene was distilled over sodium,

and all other solvents and chemical reagents were purchased from commercial sources and without further purification or treatment. All performed reactions were carried out under an atmosphere of nitrogen.

Instruments: The ^1H NMR spectra were measured on a Bruker AVANCE III 400 MHz NMR instrument at 298 K by using CDCl_3 or $\text{DMSO}-d_6$ as solvent. Chemical shifts are expressed in ppm relative to tetramethylsilane (TMS) (0 ppm). HRMS analyses were carried out on LC-QTOF-MS (G6520B/G6520B). Electronic absorption spectra were recorded on the Hitachi UH4150 UV-Visible-NIR Spectrophotometer. Fluorescence spectra were recorded on F-4600 Hitachi Fluorescence Spectrometer. The used Microplate reader was SpectraMax[®] i3x. The mentioned confocal laser scanning microscopy (CLSM) images were performed on an Olympus FV1000-IX81 CLSM and a Leica TCSSP confocal system (Leica, Germany).

4.2. The synthesis of **1b**

The methyl 4-hydroxybenzoate (0.913 g, 6 mmol) was dissolved in acetone (100 ml). Then anhydrous K_2CO_3 (2.484 g, 18 mmol) and propargyl bromide (0.857 g, 7.2 mmol) were added. The reaction refluxed overnight under nitrogen atmosphere. After it was completed, the mixture was concentrated under reduced pressure and the crude product was washed with CH_2Cl_2 and H_2O three times. The organic phase was dried over anhydrous Na_2SO_4 . After removal of Na_2SO_4 by filtration, the filtrate was concentrated under reduced pressure, then the crude product was further purified by column chromatography using CH_2Cl_2 as eluent. The product was isolated as a white solid. Yield: 1.130 g, 69.5%. ^1H NMR (400 MHz, CDCl_3) δ 8.01 (d, $J = 8.8$ Hz, 2H), 7.00 (d, $J = 8.4$ Hz, 2H), 4.75 (s, 2H), 3.89 (s, 3H), 2.55 (t, $J = 2.2$ Hz, 1H).

4.3. The synthesis of **2b**

The compound **1b** (1.620 g, 6 mmol) was dissolved in 100 ml methanol. Sodium hydroxide (1.200 g, 30 mmol) in 4 ml water was added into the reaction mixture. The reaction stirred at 80°C under N_2 atmosphere for 8 h. The volatiles was evaporated under reduced pressure. The residue was mixed with water, and then the pH of the mixture was adjusted to 1 with HCl solution. The mixture was washed with ethyl acetate and H_2O three times. The organic phase was dried over anhydrous Na_2SO_4 . After removal of Na_2SO_4 by filtration, the filtrate was concentrated under reduced pressure, then the crude product was purified by using ethyl acetate as eluent through column chromatography. The product was isolated as a white solid. Yield: 1.004 g, 95.0%. ^1H NMR (400 MHz, $\text{DMSO}-d_6$) δ 12.66 (s, 1H), 7.91 (d, $J = 7.2$ Hz, 2H), 7.07 (d, $J = 7.6$ Hz, 2H), 4.89 (s, 2H), 3.62 (d, $J = 2.5$ Hz, 1H).

4.4. The synthesis of **3b**

The ethylenediamine (1.500 g, 25 mmol) was dissolved in CH_2Cl_2 (100 ml). TsCl (0.953 g, 5 mmol) in CH_2Cl_2 (20 ml) was added dropwise over 2 h. The reaction stirred at room temperature overnight. The reaction was monitored by TLC. After the reaction was completed, the mixture was concentrated under reduced pressure. The residue was purified by column chromatography using CH_2Cl_2 : MeOH = 10:1(v/v) as eluent. The product was isolated as a white solid. Yield: 846 mg, 79.0%. ^1H NMR (400 MHz, CDCl_3) δ 7.76 (d, $J = 7.4$ Hz, 2H), 7.27 (d, $J = 7.6$ Hz, 2H), 4.80 (s, 3H), 3.04 (d, $J = 4.6$ Hz, 2H), 3.01–2.91 (m, 2H), 2.39 (s, 3H).

4.5. The synthesis of **4b**

The compound **2b** (352 mg, 2 mmol) was dissolved in anhydrous CH_2Cl_2 . EDCI (765 mg, 4 mmol) and HoBt (540 mg, 4 mmol) was added. The reaction was stirred at 0°C for 3 h. Then **3b** (450 mg, 3 mmol) and Et_3N (486 mg, 4 mmol) was added to the solution. The reaction was stirred at room temperature overnight. The mixture was washed with an aqueous HCl solution, the organic layer was dried with MgSO_4 , filtered and concentrated under reduced pressure. The mixture was further purified by column chromatography. The product was isolated as a white viscous solid. Yield 414 mg, 67.2%. ^1H NMR (400 MHz, CDCl_3) δ 7.77–7.69 (m, 4H), 7.26 (t, $J = 2.8$ Hz, 2H), 6.95 (dd, $J = 8.7, 2.2$ Hz, 2H), 6.87 (s, 1H), 4.72 (d, $J = 2.4$ Hz, 2H), 3.54 (d, $J = 5.7$ Hz, 2H), 3.17 (t, $J = 5.3$ Hz, 2H), 2.55 (t, $J = 2.5$ Hz, 1H), 2.39 (s, 3H). ^{13}C NMR (101 MHz, CDCl_3) δ 167.81, 160.09, 143.48, 136.60, 129.78, 128.98, 126.95, 126.88, 114.53, 78.00, 76.17, 55.81, 42.99, 39.90, 21.50. HRMS (ESI) m/z calcd $\text{C}_{19}\text{H}_{20}\text{N}_2\text{O}_4\text{S}$ [$\text{M}+\text{Na}$]⁺: 395.1041, found 395.1036.

4.6. The synthesis of **5b**

Compound **4b** (246 mg, 0.8 mmol) and 2-(2-(2-azidoethoxy) ethoxy) ethan-1-ol (140 mg, 0.8 mmol) was dissolved in THF (5 ml). The mixture of $\text{CuSO}_4 \cdot 5\text{H}_2\text{O}$ (15 mg) and sodium ascorbate (30 mg) were added in EtOH (0.5 ml) and water (0.5 ml). The reaction mixture stirred for 24 h at room temperature. After completed, the reaction was extracted with CH_2Cl_2 and H_2O three times and the organic layer was evaporated under reduced pressure. The residue was further purified by silica gel column chromatography using CH_2Cl_2 : MeOH = 10:1 as mobile phase. The product was isolated as colorless oily substance. Yield: 301 mg, 78.0%. ^1H NMR (400 MHz, CDCl_3) δ 7.90 (s, 1H), 7.72 (dd, $J = 8.5, 3.9$ Hz, 4H), 7.24 (d, $J = 7.9$ Hz, 2H), 7.09 (t, $J = 4.5$ Hz, 1H), 6.95 (d, $J = 8.4$ Hz, 2H), 5.30 (s, 1H), 5.23 (s, 2H), 4.57 (t, $J = 4.9$ Hz, 2H), 3.88 (t, $J = 4.9$ Hz, 2H), 3.70 (t, $J = 4.6$ Hz, 2H), 3.58 (s, 4H), 3.53 (q, $J = 7.0, 5.9$ Hz, 4H), 3.16 (t, $J = 5.4$ Hz, 2H), 2.38 (s, 3H). ^{13}C NMR (126 MHz, CDCl_3) δ 167.85, 160.72, 143.36, 143.17, 136.81, 129.72, 129.07, 126.91, 126.68, 124.70, 114.43, 72.45, 70.41, 70.09, 69.18, 61.65, 61.48, 50.31, 42.97, 39.86, 21.45. HRMS (ESI) m/z calcd for $\text{C}_{25}\text{H}_{33}\text{N}_5\text{O}_7\text{S}$ [$\text{M}+\text{Na}$]⁺: 570.1998, found: 570.1989.

4.7. The synthesis of **6b**

Erlotinib (0.944 mg, 2.4 mmol) and 2-(2-(2-azidoethoxy) ethoxy) ethan-1-ol (420 mg, 2.4 mmol) was dissolved in THF (10 ml). The mixture of $\text{CuSO}_4 \cdot 5\text{H}_2\text{O}$ (120 mg) and sodium ascorbate (240 mg) were added in EtOH (1.0 ml) and water (1.0 ml). The reaction mixture was stirred for 24 h at room temperature. After the reaction was completed, it was extracted with CH_2Cl_2 and H_2O three times and the organic layer was evaporated under reduced pressure. The residue was further purified by silica gel column chromatography using CH_2Cl_2 : MeOH = 10:1(v/v) as mobile phase. The product was isolated as yellow oily substance. Yield: 1.268 g, 93.0%. ^1H NMR (400 MHz, CDCl_3) δ 8.56 (s, 1H), 8.16 (s, 1H), 7.97 (d, $J = 8.2$ Hz, 1H), 7.92 (s, 1H), 7.66 (d, $J = 7.6$ Hz, 1H), 7.54 (s, 1H), 7.42 (d, $J = 7.9$ Hz, 1H), 7.22 (s, 1H), 4.59 (t, $J = 4.4$ Hz, 2H), 4.38–4.33 (m, 2H), 4.28–4.23 (m, 2H), 3.89 (d, $J = 4.1$ Hz, 2H), 3.84 (s, 4H), 3.81–3.77 (m, 2H), 3.66 (d, $J = 1.7$ Hz, 4H), 3.64–3.59 (m, 2H), 3.50–3.45 (m, 6H).

4.8. The synthesis of PEG-Pc

A mixture of silicon (IV) phthalocyanine dichloride (122 mg, 0.20 mmol), Triethylene glycol monomethyl ether (328 mg, 2.00 mmol), and NaH (23 mg, 1.00 mmol) in toluene (15 mL) was

kept stirring under nitrogen atmosphere at 120 °C for 24 h. After the reaction was completed, the solvents was removed under reduced pressure. And the residue was redissolved in CH₂Cl₂. Then it was purified *via* chromatography using CH₂Cl₂:MeOH (15:1) as eluent to give **PEG-Pc** as a blackish blue solid (95 mg, 54.0%). ¹H NMR (400 MHz, DMSO-*d*₆) δ 9.68 (dd, *J* = 5.6, 3.1 Hz, 8H), 8.52 (dd, *J* = 5.8, 2.9 Hz, 8H), 3.02 (d, *J* = 4.3 Hz, 10H), 2.83 (t, *J* = 4.8 Hz, 4H), 2.31 (t, *J* = 5.1 Hz, 4H), 1.59 (t, *J* = 5.1 Hz, 4H), 0.33 (t, *J* = 5.3 Hz, 4H), -2.04 (t, *J* = 5.2 Hz, 4H).

4.9. The synthesis of **EB-Pc**

A mixture of silicon (IV) phthalocyanine dichloride (122 mg, 0.20 mmol), **6b** (227 mg, 0.40 mmol), and NaH (23 mg, 1.00 mmol) in toluene (15 mL) was kept stirring under nitrogen atmosphere at 120 °C for 24 h. After the reaction was completed, the solvents was removed under reduced pressure. And the residue was redissolved in CH₂Cl₂. Then it was purified *via* chromatography using CH₂Cl₂:MeOH = 15:1 (v/v) as eluent to give **EB-Pc** as a blackish blue solid (117 mg, 35.0%). ¹H NMR (400 MHz, DMSO-*d*₆) δ 9.61 (dd, *J* = 5.7, 3.1 Hz, 8H), 9.47 (s, 2H), 8.45 (q, *J* = 4.4, 3.0 Hz, 10H), 8.06 (s, 2H), 7.88 (s, 2H), 7.85 (d, *J* = 8.1 Hz, 2H), 7.76 (s, 2H), 7.25–7.17 (m, 4H), 7.03 (d, *J* = 7.6 Hz, 2H), 4.29 (p, *J* = 4.2 Hz, 8H), 4.15 (t, *J* = 5.1 Hz, 4H), 3.77 (d, *J* = 4.8 Hz, 8H), 3.37 (d, *J* = 1.7 Hz, 12H), 3.15 (t, *J* = 5.2 Hz, 4H), 2.37 (s, 4H), 1.57 (t, *J* = 4.9 Hz, 4H), 0.33 (t, *J* = 5.1 Hz, 4H), -2.03 (t, *J* = 5.0 Hz, 4H). HRMS (ESI) *m/z* calcd for C₈₈H₈₆N₂₀O₁₄Si [M+H]⁺:1675.6480, found:1675.6425.

4.10. The synthesis of **EB-ER-Pc**

A mixture of silicon (IV) phthalocyanine dichloride (122 mg, 0.20 mmol), **6b** (114 mg, 0.20 mmol), and NaH (23 mg, 1.00 mmol) in anhydrous toluene (15 mL) was kept stirring under nitrogen atmosphere at 120 °C for 2 h. Then **5b** (110 mg, 0.2 mmol) was added and the reaction continued to stir at 120 °C for 6 h under nitrogen atmosphere. After the reaction was completed, the solvent was removed under reduced pressure. And the residue was redissolved in CH₂Cl₂. Then it was purified *via* chromatography using CH₂Cl₂:MeOH = 20:1 (v/v) as eluent to afford **EB-ER-Pc** as a blackish blue solid. Yield: 40 mg, 12.0%. ¹H NMR (400 MHz, DMSO-*d*₆) δ 9.64 (dt, *J* = 5.1, 2.2 Hz, 8H), 8.47 (dt, *J* = 5.3, 2.2 Hz, 8H), 8.26 (t, *J* = 5.9 Hz, 2H), 7.68 (dd, *J* = 7.2, 4.7 Hz, 8H), 7.65 (d, *J* = 1.8 Hz, 2H), 7.36 (d, *J* = 7.9 Hz, 4H), 7.33 (d, *J* = 1.7 Hz, 2H), 6.79 (d, *J* = 7.6 Hz, 4H), 5.76 (d, *J* = 1.7 Hz, 3H), 4.75 (s, 4H), 4.09 (t, *J* = 5.3 Hz, 4H), 3.28 (q, *J* = 6.7 Hz, 4H), 3.09 (t, *J* = 5.3 Hz, 4H), 2.88 (d, *J* = 6.6 Hz, 4H), 2.35 (d, *J* = 6.1 Hz, 10H), 1.58 (d, *J* = 5.0 Hz, 4H), 0.31 (t, *J* = 5.2 Hz, 4H), -2.05 (d, *J* = 5.3 Hz, 4H). HRMS (ESI) *m/z* calcd for C₈₅H₈₃N₁₉O₁₄Si [M]⁺:1653.5857, found:1653.5073.

4.11. Cell lines and culture conditions

All employed cell lines were from the China Center for Type Culture Collection (CCTCC). The cell line A549 cells (human lung carcinoma), PC-9 cells (human lung adenocarcinoma) and HELF cells (human embryonic lung fibroblast) were incubated with DMEM containing 10% fetal bovine serum (FBS). All cells were cultured at 37 °C under 5% CO₂ atmosphere.

4.12. Dark cytotoxicity assay

The cells were seeded into a 96-well cell culture plate at a density of 6000 cells per well and cultured at 37 °C under 5% CO₂ atmosphere overnight. **EB-ER-Pc**, **EB-Pc**, and **PEG-Pc** were dissolved into DMF with 5% CEL as the stock solution. After that, the compounds were further diluted into different concentrations by

using the fresh medium. A series of different concentrations of compounds in 100 μL medium were successively added into the 96-well cell culture plate. After a 24 h incubation, the old medium with extra drugs outside the cells was removed and replaced with fresh medium. Then the pre-prepared MTT solution (10 μL, 5 mg/mL in PBS) was added into the per well and the cells continued to be further incubated for an extra 4 h. The old medium was discarded carefully and 100 μL DMSO was added into per well. The absorbance at 490 nm was monitored by a Microplate reader. The survival curves were plotted as a concentration dependence curve of the drug.

4.13. Colocalization experiments

The cells were seeded in 20 mm confocal dishes and incubated overnight at 37 °C under 5% CO₂ atmosphere. Then the cells were incubated with **EB-ER-Pc**, **EB-Pc**, and **PEG-Pc** (all at 1.0 μM) respectively for 24 h. After washing out the excess compound with PBS three times, the cells were stained with 2 μM Mito-Tracker green (Nanjing KeyGen BioTECH) for 30 min, 2 μM Lyso-Tracker Green (Nanjing KeyGen BioTECH) for 60 min or 1.0 μM ER-Tracker Green (Invitrogen) for 60 min at 37 °C respectively. After that, the cells were rinsed with PBS three times and taken by CLSM.

4.14. Intracellular ROS measurements

Approximately 1.0 × 10⁵ A549 cells were seeded into 20 mm confocal culture dishes and incubated overnight at 37 °C under 5% CO₂. Then the cells were treated with 0, 10, 50, 100 or 500 nM **EB-ER-Pc** for 24 h respectively. After incubation, the old medium containing drugs was discarded and the cells were rinsed with PBS three times, and then the culture medium with DCFH-DA (Beyotime, S0033) in DMEM (10 μM) was added and the cells were incubated with the dye for 30 min again. After incubation, the old medium with the excess fluorescence probe was discarded and then washed three times with PBS again followed by LED light illumination (λ = 670 nm, 12.5 mWcm⁻² 1.5 J cm⁻²) for 2 min. The intracellular fluorescence of DCF was revealed by CLSM. (excitation/emission: 488/525 nm).

The A549 cells were seeded onto a 96-well plate at a density of 1.0 × 10⁵ cells/ml and cultured overnight. Then fresh medium containing different concentrations of conjugates (10, 25, 50, 100, 500 nM) was added and the cells were incubated with drugs for 24 h in the dark. After washing out the excess compounds with PBS three times, the cells were treated with 100 μL DCFH-DA in DMEM (10 μM) to incubate for 30 min. The old medium with the excess fluorescence probe was discarded and then washed three times with PBS again followed by LED light illumination (λ = 670 nm, 12.5 mWcm⁻² 1.5 J cm⁻²) for 2 min. Then the cells were lysed by using pre-prepared 1% SDS (120 μL) for 20 min at a table concentrator, and then the fluorescence of DCF was measured and recorded by a microplate reader (excitation/emission: 488/525 nm).

4.15. Analysis of mitochondrial membrane potential (MMP)

Approximately 1.0 × 10⁵ A549 cells were seeded in 20 mm confocal culture dishes and cultured overnight at 37 °C under 5% CO₂ atmosphere to adhere. Then the cells were incubated with different concentrations of **EB-ER-Pc**, **EB-Pc**, and **PEG-Pc** (0, 1, 10, 25, and 100 nM) for 24 h, followed by LED light illumination for 2 min. After 24 h of treatment, the cells were washed three times with PBS carefully and stained with a 6 μM JC-1 dye (Nanjing KeyGen BioTECH) to measure the MMP according to the directions. After 30 min later, the fluorescence intensity of the cells was measured by CLSM with a 488 nm laser and a 546 nm laser.

4.16. Detection of intracellular calcium level

The A549 cells were seeded onto a 96-well plate at a density of 1.0×10^5 cells/ml and cultured overnight at 37°C under 5% CO_2 atmosphere. Then fresh medium containing different concentrations of the conjugates (10, 25, 50, 100, 500 nM) was added, and cells incubated with drugs for 24 h in the dark. After PDT treatment, the cells were washed three times by using PBS and then the fluorescence probe Fluo-3 AM (Sigma-Aldrich, 39294) in 100 μL DMEM (10 μM) was added into each well to incubate for 30 min. The old medium with excess fluorescence dye outside the cells was discarded and washed three times with PBS again. Finally, the cells were lysed by using pre-prepared 1% SDS (120 μL) for 20 min at a table concentrator, and then the fluorescence was measured and recorded by a microplate reader (excitation/emission: 488 nm/535 nm).

4.17. In vitro photocytotoxicity assay

Cells were seeded into a 96-well cell culture plate with the density of 6.0×10^4 cells/ml and cultured overnight at 37°C with 5% CO_2 to adherence. **ER-EB-Pc**, **EB-Pc**, and **PEG-Pc** were diluted into DMF (contain 5% CEL). After that, the compounds were further diluted into different concentrations with the fresh medium. A series of different concentrations of compounds in 100 μL medium were successively added into the 96-well cell culture plate. After a 24 h incubation, the old medium with extra drugs outside the cells was removed and replaced by fresh medium. And then the cells were exposed to LED light illumination ($\lambda = 670$ nm, 1.5 J cm^{-2}) for 2 min. The cells after irradiation were further cultured for 24 h again. After a 24 h incubation, the old medium was discarded and replaced by fresh medium. Then the pre-prepared MTT solution (10 μL , 5 mg/mL in PBS) was added into the per well and the cells continued to be further incubated for an extra 4 h. The old medium was removed carefully and 100 μL DMSO was added into the per well. The absorbance at 490 nm was recorded by a Microplate reader. The survival curves were plotted as a concentration dependence curve of the drug, and IC_{50} values were calculated.

Approximately 1.0×10^5 A549 cells were seeded on 20 mm confocal culture dishes and incubated overnight at 37°C under 5% CO_2 atmosphere. Then the cells were treated with 0, 1, 10, 25 or 100 nM **EB-ER-Pc** for 24 h respectively. After incubation, the old medium with extra drugs outside the cells was discarded and the cells were rinsed with PBS three times. Then the double staining reagent calcein AM and PI (Nanjing KeyGen BioTECH) in DMEM (all at 5 μM) was added and further incubated with the cells for 30 min again. After incubation, the intracellular fluorescence of calcein AM and PI was observed by CLSM (Calcein AM: $\lambda_{\text{exc}} = 488$ nm, $\lambda_{\text{em}} = 525$ nm; PI: $\lambda_{\text{exc}} = 530$ nm, $\lambda_{\text{em}} = 620$ nm).

Acknowledgments

This work was supported by the Natural Science Foundation of China (Project No. 81703345, 81803346, 51672046), the National Health and Family Planning Commission jointly established a scientific research fund (Project No. WKJ2016-2-14), and the Natural Science Foundation of Fujian Province (Project No. 2015Y0086, 17J05021).

Appendix A. Supplementary data

Supplementary data to this article can be found online at <https://doi.org/10.1016/j.ejmech.2019.111625>.

References

- [1] J. Mu, J. Lin, P. Huang, X. Chen, Development of endogenous enzyme-responsive nanomaterials for theranostics, *Chem. Soc. Rev.* 47 (2018) 5554–5573.
- [2] X. Ai, M. Hu, Z. Wang, L. Lyu, W. Zhang, J. Li, H. Yang, J. Lin, B. Xing, Enhanced cellular ablation by attenuating hypoxia status and reprogramming tumor-associated macrophages via NIR light-responsive upconversion nanocrystals, *Bioconjug. Chem.* 29 (2018) 928–938.
- [3] W. Fan, P. Huang, X. Chen, Overcoming the Achilles' heel of photodynamic therapy, *Chem. Soc. Rev.* 45 (2016) 6488–6519.
- [4] P. Agostinis, K. Berg, K.A. Cengel, T.H. Foster, A.W. Girotti, S.O. Gollnick, S.M. Hahn, M.R. Hamblin, A. Juzeniene, D. Kessel, M. Korbelik, J. Moan, P. Mroz, D. Nowis, J. Piette, B.C. Wilson, J. Golab, Photodynamic therapy of cancer: an update, *CA A Cancer J. Clin.* 61 (2011) 250–281.
- [5] P. Di Mascio, G.R. Martinez, S. Miyamoto, G.E. Ronsein, M.H.G. Medeiros, J. Cadet, Singlet molecular oxygen reactions with nucleic acids, lipids, and proteins, *Chem. Rev.* 119 (2019) 2043–2086.
- [6] H. Wang, J. Chang, M. Shi, W. Pan, N. Li, B. Tang, A dual-targeted organic photothermal agent for enhanced photothermal therapy, *Angew. Chem. Int. Ed. Engl.* 58 (2019) 1057–1061.
- [7] Imaging and Photodynamic Therapy: Mechanisms, Monitoring, and Optimization, 2010.
- [8] X. Li, S. Lee, J. Yoon, Supramolecular photosensitizers rejuvenate photodynamic therapy, *Chem. Soc. Rev.* 47 (2018) 1174–1188.
- [9] S. Verma, G.M. Watt, Z. Mai, T. Hasan, Strategies for enhanced photodynamic therapy effects, *Photochem. Photobiol.* 83 (2007) 996–1005.
- [10] X. Li, B.-D. Zheng, X.-H. Peng, S.-Z. Li, J.-W. Ying, Y. Zhao, J.-D. Huang, J. Yoon, Phthalocyanines as medicinal photosensitizers: developments in the last five years, *Coord. Chem. Rev.* 379 (2019) 147–160.
- [11] M.R. Ke, S.L. Yeung, D.K. Ng, W.P. Fong, P.C. Lo, Preparation and in vitro photodynamic activities of folate-conjugated distyryl boron dipyrromethene based photosensitizers, *J. Med. Chem.* 56 (2013) 8475–8483.
- [12] F.L. Zhang, Q. Huang, K. Zheng, J. Li, J.Y. Liu, J.P. Xue, A novel strategy for targeting photodynamic therapy. Molecular combo of photodynamic agent zinc(II) phthalocyanine and small molecule target-based anticancer drug erlotinib, *Chem Commun (Camb)* 49 (2013) 9570–9572.
- [13] X. Ai, C.J. Ho, J. Aw, A.B. Attia, J. Mu, Y. Wang, X. Wang, Y. Wang, X. Liu, H. Chen, M. Gao, X. Chen, E.K. Yeow, G. Liu, M. Olivo, B. Xing, In vivo covalent cross-linking of photon-converted rare-earth nanostructures for tumour localization and theranostics, *Nat. Commun.* 7 (2016) 10432.
- [14] M.K. Yu, J. Park, S. Jon, Targeting strategies for multifunctional nanoparticles in cancer imaging and therapy, *Theranostics* 2 (2012) 3–44.
- [15] X. Zhao, Y. Huang, G. Yuan, K. Zuo, Y. Huang, J.-J. Chen, J. Li, J. Xue, A novel tumor and mitochondria dual-targeted photosensitizer showing ultra-efficient photodynamic anticancer activities, *Chem. Commun.* 55 (2018) 866–869.
- [16] F.L. Zhang, M.R. Song, G.K. Yuan, H.N. Ye, Y. Tian, M.D. Huang, J.P. Xue, Z.H. Zhang, J.Y. Liu, A molecular combination of zinc(II) phthalocyanine and tamoxifen derivative for dual targeting photodynamic therapy and hormone therapy, *J. Med. Chem.* 60 (2017) 6693–6703.
- [17] M. Lismont, L. Dreesen, S. Wuttke, Metal-organic framework nanoparticles in photodynamic therapy: current status and perspectives, *Adv. Funct. Mater.* 27 (2017) 1606314.
- [18] M. Srinivasarao, P.S. Low, Ligand-targeted drug delivery, *Chem. Rev.* 117 (2017) 12133–12164.
- [19] W.H. Chen, G.F. Luo, X.Z. Zhang, Recent advances in subcellular targeted cancer therapy based on functional materials, *Adv. Mater.* 31 (2019), e1802725.
- [20] H. Wang, Z. Gao, X. Liu, P. Agarwal, S. Zhao, D.W. Conroy, G. Ji, J. Yu, C.P. Jaroniec, Z. Liu, X. Lu, X. Li, X. He, Targeted production of reactive oxygen species in mitochondria to overcome cancer drug resistance, *Nat. Commun.* 9 (2018) 562.
- [21] H.S. Jung, J.H. Lee, K. Kim, S. Koo, P. Verwilt, J.L. Sessler, C. Kang, J.S. Kim, A mitochondria-targeted cyanine-based photothermogenic photosensitizer, *J. Am. Chem. Soc.* 139 (2017) 9972–9978.
- [22] S. Chakraborty, B.K. Agrawalla, A. Stumper, N.M. Vegi, S. Fischer, C. Reichardt, M. Kogler, B. Dietzek, M. Feuring-Buske, C. Buske, S. Rau, T. Weil, Mitochondria targeted protein-ruthenium photosensitizer for efficient photodynamic applications, *J. Am. Chem. Soc.* 139 (2017) 2512–2519.
- [23] Q. Hu, M. Gao, G. Feng, B. Liu, Mitochondria-targeted cancer therapy using a light-up probe with aggregation-induced-emission characteristics, *Angew. Chem. Int. Ed. Engl.* 53 (2014) 14225–14229.
- [24] L.F. Yousif, K.M. Stewart, S.O. Kelley, Targeting mitochondria with organelle-specific compounds: strategies and applications, *Chembiochem* 10 (2009) 1939–1950.
- [25] Z. Feng, H. Wang, S. Wang, Q. Zhang, X. Zhang, A.A. Rodal, B. Xu, Enzymatic assemblies disrupt the membrane and target endoplasmic reticulum for selective cancer cell death, *J. Am. Chem. Soc.* 140 (2018) 9566–9573.
- [26] S. Banerjee, W. Zhang, Endoplasmic reticulum: target for next-generation cancer therapy, *Chembiochem* 19 (2018) 2341–2343.
- [27] M. Dong, X.Z. Xiao, Z.G. Su, Z.H. Yu, C.G. Qian, J.H. Liu, J.C. Zhao, Q.D. Shen, Light-induced ROS generation and 2-DG-activated endoplasmic reticulum stress by antitumor nanosystems: an effective combination therapy by

- regulating the tumor microenvironment, *Small* 15 (2019), e1900212.
- [28] H. Xiao, C. Wu, P. Li, B. Tang, Simultaneous fluorescence visualization of endoplasmic reticulum superoxide anion and polarity in myocardial cells and tissue, *Anal. Chem.* 90 (2018) 6081–6088.
- [29] Y.L. Pak, S.J. Park, G. Song, Y. Yim, H. Kang, H.M. Kim, J. Bouffard, J. Yoon, Endoplasmic reticulum-targeted ratiometric N-heterocyclic carbene borane probe for two-photon microscopic imaging of hypochlorous acid, *Anal. Chem.* 90 (2018) 12937–12943.
- [30] S. Xu, H.W. Liu, X.X. Hu, S.Y. Huan, J. Zhang, Y.C. Liu, L. Yuan, F.L. Qu, X.B. Zhang, W. Tan, Visualization of endoplasmic reticulum aminopeptidase 1 under different redox conditions with a two-photon fluorescent probe, *Anal. Chem.* 89 (2017) 7641–7648.
- [31] J.T. Hou, H.S. Kim, C. Duan, M.S. Ji, S. Wang, L. Zeng, W.X. Ren, J.S. Kim, A ratiometric fluorescent probe for detecting hypochlorite in the endoplasmic reticulum, *Chem. Commun. (Camb)* 55 (2019) 2533–2536.
- [32] J.T. Lau, P.C. Lo, X.J. Jiang, Q. Wang, D.K. Ng, A dual activatable photosensitizer toward targeted photodynamic therapy, *J. Med. Chem.* 57 (2014) 4088–4097.
- [33] B.Y. Zheng, X.Q. Yang, Y. Zhao, Q.F. Zheng, M.R. Ke, T. Lin, R.X. Chen, K.K.K. Ho, N. Kumar, J.D. Huang, Synthesis and photodynamic activities of integrin-targeting silicon(IV) phthalocyanine-cRGD conjugates, *Eur. J. Med. Chem.* 155 (2018) 24–33.
- [34] M. David Maree, Nina Kuznetsova, T. Nyokong, Silicon octaphenoxyphthalocyanines: photostability and singlet oxygen quantum yields, *J. Photochem. Photobiol. A Chem.* 140 (2001) 117–125.
- [35] P.R. Ogilby, Singlet oxygen: there is indeed something new under the sun, *Chem. Soc. Rev.* 39 (2010) 3181–3209.
- [36] Y. Ge, X. Weng, T. Tian, F. Ding, R. Huang, L. Yuan, J. Wu, T. Wang, P. Guo, X. Zhou, A mitochondria-targeted zinc(ii) phthalocyanine for photodynamic therapy, *RSC Adv.* 3 (2013) 12839–12846.
- [37] J. Morgan, A.R. Oseroff, Mitochondria-based photodynamic anti-cancer therapy, *Adv. Drug Deliv. Rev.* 49 (2001) 71–86.
- [38] R. Sano, J.C. Reed, ER stress-induced cell death mechanisms, *Biochim. Biophys. Acta* 1833 (2013) 3460–3470.